Flow control on a bluff body using dielectric barrier discharge plasma actuators

Zongnan Chen *
The Hong Kong Polytechnic University, Hong Kong, People's Republic of China

Lu Shen†
The Hong Kong Polytechnic University, Hong Kong, People's Republic of China

Chih-Yung Wen‡
The Hong Kong Polytechnic University, Hong Kong, People's Republic of China

In this study, a traditional dielectric barrier discharge (DBD) plasma actuator and plasma streamwise vortex generators (PSVGs) are installed on a bluff body to control the wake fluctuations. Experiments are conducted in a wind tunnel with a chord Reynolds number of 5000. Particle image velocimetry (PIV) and hot-wire measurements are used to obtain the details of the flow fields. The results show that both DBD and PSVG actuations clearly reduce the size of the recirculation bubble regions, and significantly suppress the wake fluctuations. A comparison of the traditional DBD and PSVG cases shows that PSVGs have better control performance on the reduction of the recirculation bubble sizes and the Karman vortex shedding frequency in the wake at low speed. Specifically, the PSVGs have a strong three-dimensional effect on the entire flow field and generate streamwise vorticities that interact with the shear flow over the bluff body. The local flow separations are thereby suppressed considerably. The induced streamwise vorticities are further entrained downstream by the ambient freestream, which consequently reduces the recirculation bubble behind the bluff body and suppresses the wake fluctuations. These results suggest that PSVGs are promising devices for conducting flow control in bluff body wakes at low speed.

Nomenclature

Re	=	Reynolds number
U_∞	=	freestream velocity, m/s
U	=	horizontal velocity profile of selected section, m/s
V	=	vertical velocity profile of selected section, m/s

*Research Assistant, Department of Mechanical Engineering, zongnan.chen@connect.polyu.hk

†Research Fellow, currently in School of Mechanical and Aerospace Engineering, Nanyang Technological University, Singapore, shenlu1000@gmail.com

‡Professor, Department of Mechanical Engineering, cywen@polyu.edu.hk. Associate Fellow AIAA.

d = the diameter of the circular nose, mm

f = frequency in fast Fourier transform, Hz

x, y, z = coordinate measured from back surface of bluff body model

λ = the spanwise distance between two adjacent electrodes, mm

$\overline{\omega_x}$ = time-averaged vorticity in y-z planes, s^{-1}

I. Introduction

Vortex shedding is commonly observed when fluids flow past a bluff body. The vortex streets are formed through the interaction of the two separated shear layers via entrainment.[1, 2] The growing vortex is ultimately cut off by the entrainment of the vorticity and shed from the bluff body. For a short body with a round nose, the vortex shedding process is not only affected by the geometry of the trailing edges, but is also related to the flow separation at the round nose.[3–5] Due to the periodic oscillation, which adversely affects the flow structure by shedding vortices, the flow instability increases in the wake. Hence, suppression of the vortex shedding can help reduce the pernicious effects of the periodic oscillation.

In recent years, active flow control via dielectric barrier discharge (DBD) plasma actuators has attracted significant attention because of its flexibility, high efficiency,and fast response.[6–8] Do et al[9] used DBD actuators to delay flow separation at the round-cornered trailing edge of a bluff body. Bhattacharya[10] et al conducted experiments to optimize the spatial-forcing-wavelength of a DBD actuator array which generated three-dimensional flows to control the wake of a circular cylinder. More recently, plasma streamwise vortex generators (PSVGs) have been designed to generate streamwise vorticities via a series of exposed electrodes aligned with the mean flow direction.[11–13] PSVGs have been applied to cylinder wake control, airfoil control, and boundary layer control on a flat plate. Jukes et al [11] compared two streamwise oriented DBD plasma actuators on a NACA 4418 airfoil for flow separation control, which created counterrotating and corotating vortex arrays. The counterrotating vortex actuator was found performing slightly better than the other one. Wicks et al [12] studied the influences of some parameters on streamwise vorticity generation and provided the guidance for optimizing the PSVGs design based on the vorticity transport equation. The guidance was also experimentally validated. Kelley et al [13] presented the design and scaling of PSVGs in a variable pressure gradient environment and conducted measurements in the boundary layer on the suction surface of a V-22 wing model for separation control.

However, the underlying control mechanisms of PSVGs are not well understood. In addition, the potential of PSVGs for flow control in bluff body wakes has not been sufficiently explored. In this study, experiments were conducted to compare the performance of the traditional DBD actuators and PSVGs in controlling the flow in the bluff body wake and determine the corresponding control mechanisms. PIV experiments in streamwise and spanwise flows of PSVGs

were conducted to construct the three-dimensional flow structures.

II. Experimental Setup

The experiments were conducted in a closed-loop low-speed wind tunnel with a test section of 2.4 m (length) × 0.6 m (width) × 0.6 m (height). In the experiments, the freestream velocity U_∞ was set as 1.67 ms^{-1}, resulting in a Reynolds number of 5000 based on the chord length of the bluff body. The corresponding turbulence intensity of the freestream was less than 0.4%. The bluff body model comprised an acrylic circle-square cylinder (see Fig.1) with a round nose radius of 15 mm, square body width of 30 mm, and overall spanwise length of 600 mm. Notably, the robotic airships with a blunt-nosed shape would be one of the practical applications of the bluff body shape under consideration[14, 15]. These air vehicles, generally operated at low speed and low altitude, are potential platforms for aerial exploration, monitoring, and surveillance. Some structures in the airship, such as the gondola and the tail fin, also share the similar bluff body shape. Plasma actuators were installed symmetrically on the upper and lower surfaces in the central part of the model, with an effective spanwise length of 120 mm. Two types of plasma actuators were examined: a traditional SDBD actuator (Fig.1(a)) and PSVGs (Fig.1(b)). The electrodes were made of copper film with a thickness of 0.025 mm and the dielectric layer was made of acrylic with a thickness of 1 mm. The widths of the exposed electrodes and insulated electrodes were 3.2 mm and 16 mm, respectively. For the traditional DBD plasma actuator, the gap between the exposed electrode and the insulated electrode was set at 2 mm for optimal performance (Fig.1(a)).[16] For the PSVGs, the spanwise distance between two adjacent electrodes was 25.4 mm (λ) which is the optimal value suggested by Wicks et al[12, 13]. There was a 2 mm gap between the exposed electrodes and insulated electrodes. Overall, five sets of PSVGs were arranged along the spanwise direction. The actuators were driven by a 20 kHz sine waveform AC power supply with a peak-to-peak voltage of 11 kV. Because the exciting frequency of the actuators was much higher than the natural vortex shedding frequencies, the controls were considered to be continuous.

For the PIV measurement, the entire wind tunnel was seeded with olive oil droplets using a TSI 9307-6 aerosol generator. The normal diameter of the droplets was 1 μm. The oil droplets were lit by a 532 nm dual-pulse laser (with a pulse energy of 600 mJ), and the corresponding images were acquired by a CCD camera with a resolution of 2080 × 2080 pixels. Five y-z observation planes were selected, located from $x = -20$ mm (the upstream edge of the PSVGs) to $x = 20$ mm with an increment of 10 mm, as shown in Fig.1(c). Two x-y observation planes were also chosen, at $z = 0$ (Section A) and $z = 12.7$ mm (Section B) , corresponding to the symmetric planes between the exposed electrodes and insulated electrodes, respectively (Fig.1(d)). The experiment for each case was repeated for 3 times. The data analysis was performed using an adaptive PIV correlation (Dantec DynamicStudio). The velocity measurement uncertainty was less than 1.25% [17] and the uncertainty of the vorticity estimated (defined as $\overline{\omega_x} \equiv \overline{\partial v_z/\partial y - \partial v_y/\partial z}$) was 0.25%. [18] Hot-wire anemometry (Dantec miniature wire probe, straight (55P11)) was used to acquire the fluctuations of the streamwise velocity component at a location of $x = 120$ mm, $y = 30$ mm, and $z = 0$ mm, with a sampling frequency of

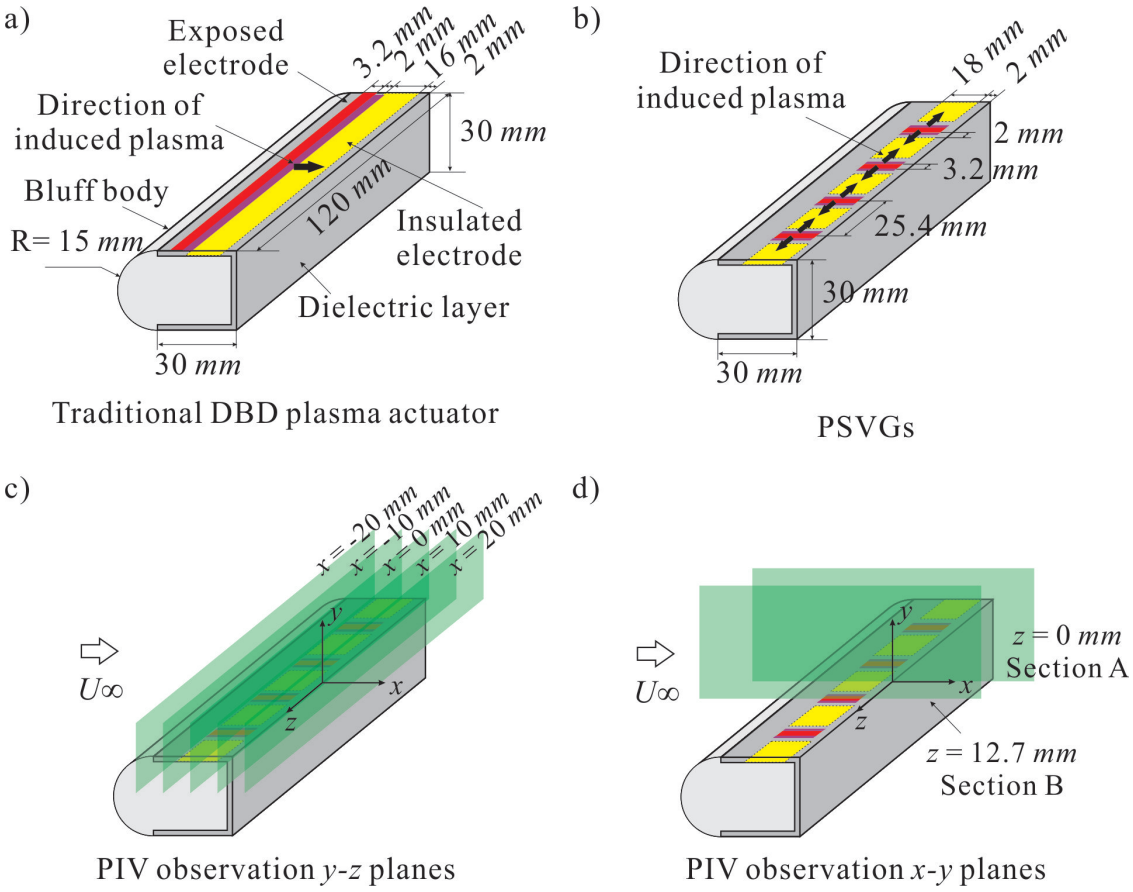

Fig. 1 Schematics of the bluff body models with a) the traditional DBD plasma actuator and b) PSVGs; c) *y*-*z* planes and d) *x*-*y* planes for the PIV measurement.

2000 Hz and the uncertainty was less than 2%.

III. Results and Discussions

A. Induced Flow in Quiescent Air

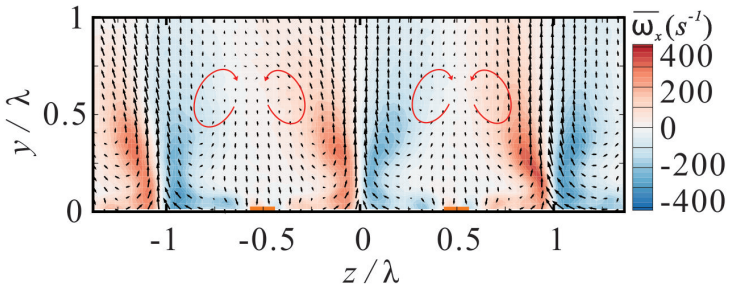

Fig. 2 Time-averaged vorticity contours with velocity vectors of the flow induced by PSVGs (x = −10 mm) in quiescent air.

In quiescent air, the traditional DBD plasma actuators generate a wall-jet-like induced flow on the model surface[19], while PSVGs induce pairs of counter-rotating streamwise vortices near the surface.[12] Fig.2 shows an example of the PSVG induced flow along the y-z plane at $x = -10$ mm. As observed, wall-jet-like flows are induced on the model surface, moving from the exposed electrodes towards the insulated electrodes. Pairs of opposite induced flows (see the red arrows in Fig.2) meet at the middle of the insulated electrodes and then become strong shear flows towards the upward section. Finally, these shear flows roll into pairs of counter-rotating vortices, which are moving in the streamwise direction.

B. Wake and Separation

The time-averaged wake structures in the x-y planes with/without controls are presented in Fig.3. For the plasma off cases (see Fig.3(b)(f)(j)), the recirculation bubble region is very large, and the two separation streamlines reattach at x/d = 2.8, forming a saddle point. Here, d is the diameter of the circular nose. The length of the recirculation bubble is defined, therefore, by the distance from the corresponding saddle point to the back surface of bluff body. Meanwhile, the width of the recirculation bubble normalized by d is defined by the maximum lateral distance between two separation streamlines from the model. The width of the recirculation bubble is about 1.5 for the plasma off cases (marked in Fig.3(b)(f)(j)). The results show that the influence of installation of different actuators on the flow is very limited. The experiment for each case was repeated for 3 times, as shown in Figure 4. Good experimental repeatability is observed. When controlled by the DBD actuator (see Fig.3 (d)), the recirculation bubble region shrinks, the reattachment point, which is considered to be the point at the end of the recirculation zone moves upstream to x/d = 1.75, and the width of the wake reduces to 1.25. In the PSVGs case, reductions of the recirculation bubble region are also observed in section A (Fig.3(h)) and section B (Fig. 3(l)). The length of the recirculation bubble reduces to 1.2 for section A and 1.0 for section B, respectively (see Figure 4). The decrease of recirculation bubble length is significant compared with that in the DBD case. Also, a noticeable difference in the width of the recirculation bubble between the DBD case and PSVGs case can be seen in Figure 4. The width of the recirculation bubble reduces to 0.9 for section A and 1.0 for section B, respectively. This result implies that the PSVGs have a strong three-dimensional effect on the flow field.

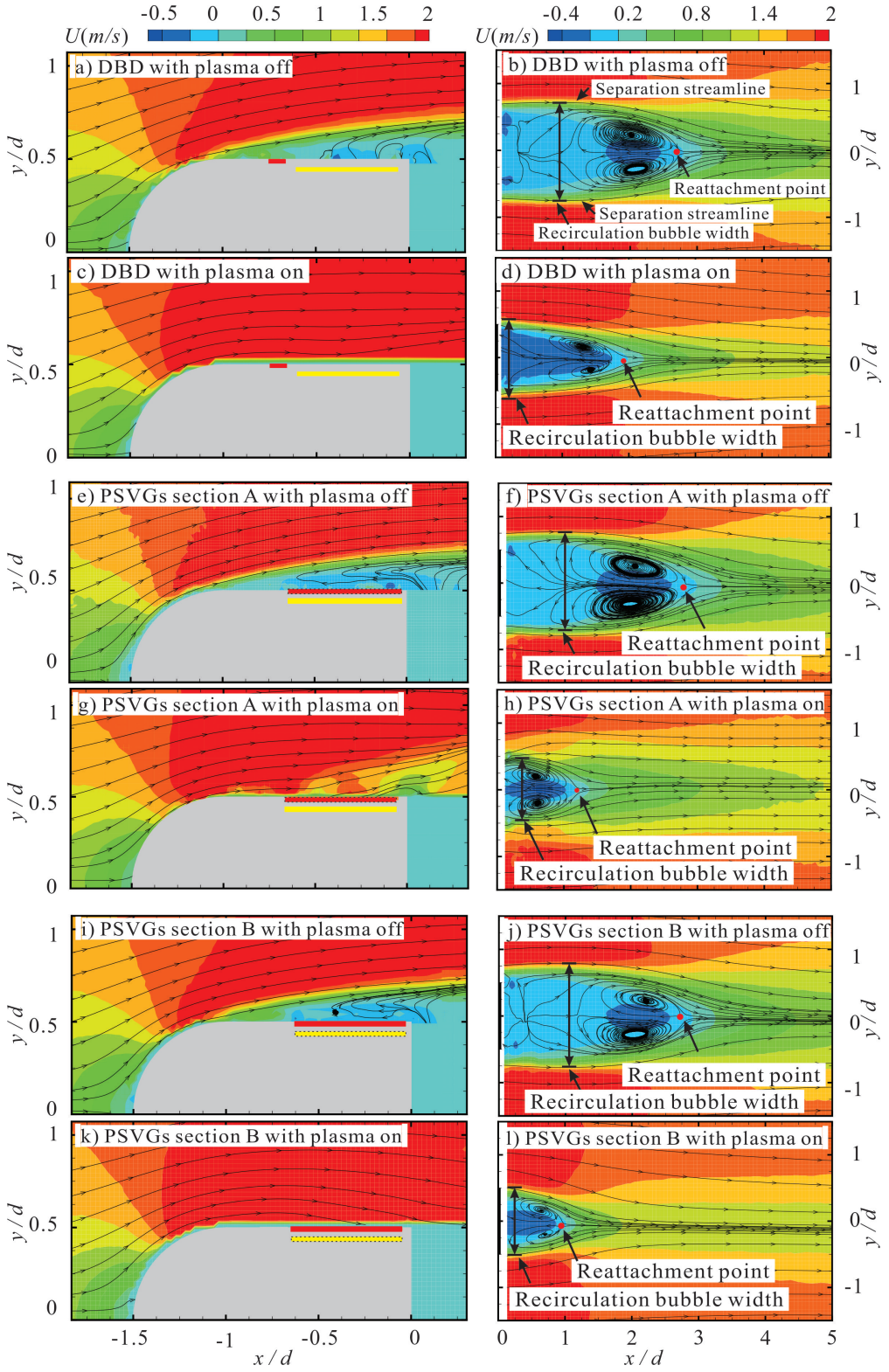

Fig. 3 **Time-averaged flow structures over the bluff body and wake structures in the *x*-*y* plane: a) & b)DBD with plasma off; c) & d) DBD with plasma on ; e) & f) PSVGs section A with plasma off; g) & h) PSVGs section A with plasma on; i) & j) PSVGs section B with plasma off; k) & l) PSVGs section B with plasma on.**

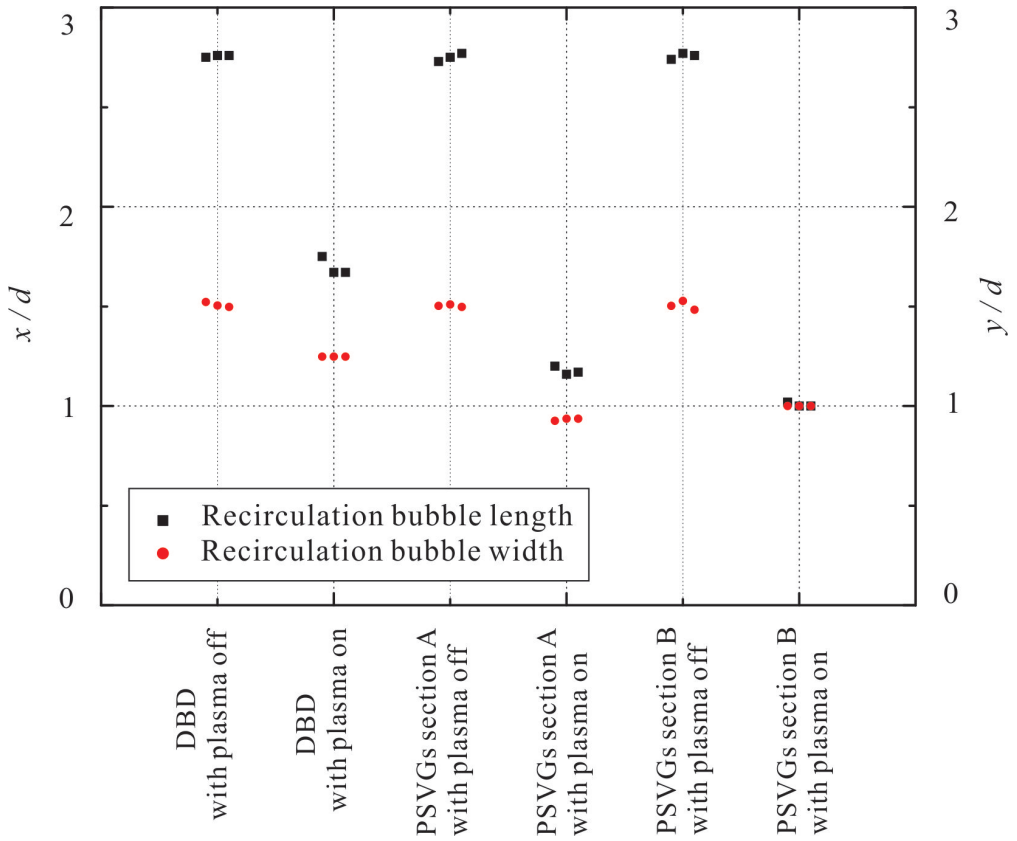

Fig. 4 The length (x/d) and width (y/d) of the recirculation bubble for different cases.

To understand the underlying control mechanisms, the flow field on the surface of the bluff body was investigated. The streamlines and streamwise velocity (U-component) contours are shown in Fig.3. For the plasma off cases shown in Fig.3(a)(e)(i),the flow separates on the round surface, and a recirculation region forms on the upper surface (known from the streamlines). Because the chord length is insufficiently long, the separated shear flows do not reattach to the surfaces. In Fig.3(c), the separation is suppressed due to the excitation of the DBD plasma actuator. With the PSVGs, the flow separations are suppressed in both section A (Fig.3(g)) and section B (Fig.3(k)). Both DBD and PSVG actuators are effective to suppress the separation because the induced flow caused by actuators can transfer the momentum into the boundary layer downstream of the separation point and increase the resistance from separation consequently[9]. However, with the PSVGs, the up-wash flow moves up fluid with lower U-momentum from the wall in section A and the downwash flow brings fluid with higher U-momentum from the freestream toward the wall in section B (see Fig.3), which yields a more effective momentum mixing and a greater reduction of the recirculation bubble size than with the DBD actuator (see Fig.4).

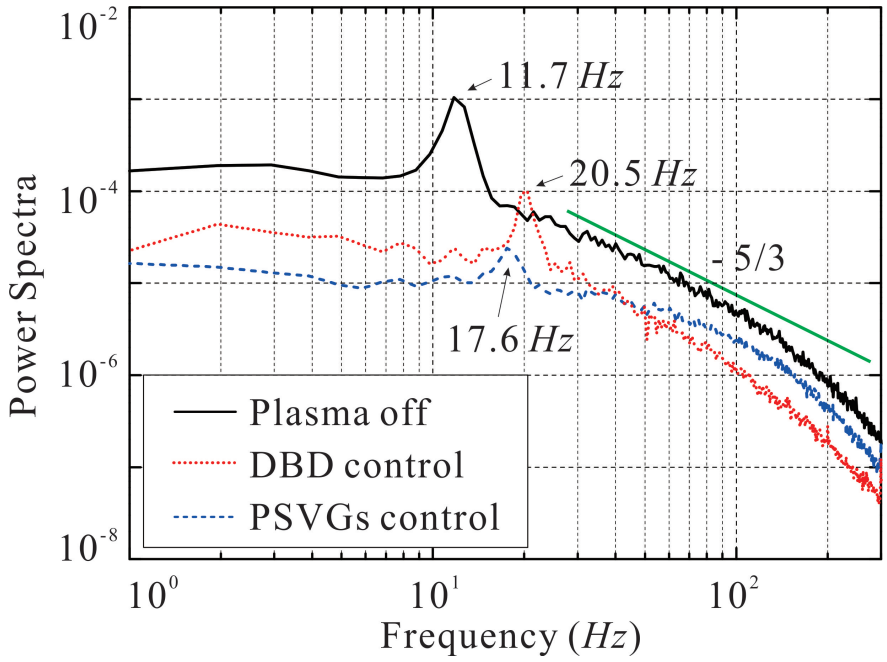

Fig. 5 Power spectra of the velocity fluctuations in the wake.

The temporal velocity fluctuations in the wake (x/d = 4, y/d = 1) were acquired using hot-wire measurements. FFT analysis was conduced to obtain the frequency power spectra. The results of the plasma-off case, DBD case and PSVGs case are shown in Fig.5. In the plasma-off case, the dominant spectra peak at f = 11.7 Hz represents the natural frequency of the Karman vortex shedding from the separated flow region. With the traditional DBD control, the dominant spectra peak increases to f = 20.5 Hz, and the overall power spectrum decreases dramatically. For the PSVG controls, the power spectra of the dominant peak are significantly lower than those of the DBD control at lower frequencies (f = 17.6 Hz). Hence, both the DBD and PSVG actuators affect the vortex shedding frequency and suppresses the fluctuation level in the bluff body wake[4, 5]. The increase of dominant vortex shedding frequency is due to the different degree of flow acceleration over the bluff body by the DBD and PSVG actuators[3].

C. Crossflow Interaction

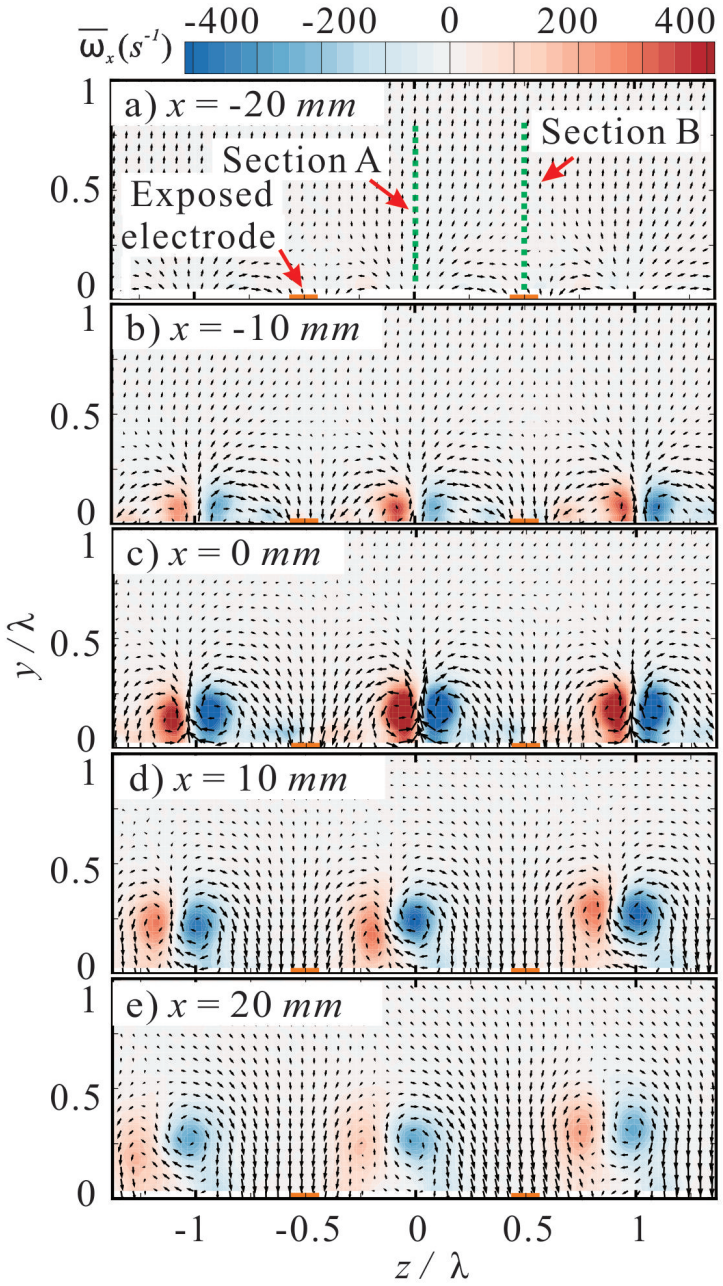

Fig. 6 Time-averaged velocity vectors and vorticity contours of the flow along the y-z planes with PSVGs: a) x = −20 mm; b) x = −10 mm; c) x = 0 mm; d) x = 10 mm; and e) x = 20 mm.

Fig.6 shows the evolution of the pairs of counter-rotating vortices (uncertainty was 0.25%) induced by the PSVGs. The x-y planes are from x = −20 mm to x = 20 mm. Fig.6(a) shows that streamwise vortices are not formed at the front edge of the actuator. The velocity vector map shows that the freestream in section B is sucked towards the exposed electrodes. Therefore, the local flow remains attached to the model surface. Near section A, neighboring flows are

entrained to form crossflows, and the local flow is thereby also attached to the model surface. Thus, the separations are suppressed at this location (also known from Fig.4). At $x = -10$ mm, pairs of vorticity concentrations are observed close to the model surface, which indicates that pairs of induced counter-rotating vortices are formed at this x location. As known from the velocity vectors, the V-component in section A is positive and its magnitude is relatively large. Hence, the approaching freestream separates from the model surface at this location. However, due to the existence of the streamwise vortices, no spanwise recirculation region forms in this region (as in Fig.3(g)). In section B, the V-component is negative because the ambient freestream is entrained towards the model surface, and separations thereby do not occur in this region (as in Fig.3(k)). At the trailing edge $x = 0$, the magnitude and size of these induced vorticity concentrations increase significantly, while the positions of the vorticity concentrations move upward. The positive V-component in section A and negative V-component in section B are also enlarged due to the momentum feeding from the actuator. Thus, the width of the wake in section A is much larger than that in section B (also seen in Fig.3). After the trailing edge, the streamwise vorticities quickly reduce and the vortices breakdown in the wake due to the insufficient momentum feeding. These induced streamwise vortices interact with the freestream and suppress the formation of spanwise vortices in the wake.

IV. Conclusion

In summary, experiments were conducted to compare the performance of a traditional DBD plasma actuator and PSVGs in controlling the flow in a bluff body wake, and explore the underlying control mechanisms. The results show that the both plasma actuators suppress the flow separation on the bluff body, reduce the size of the wake, and decrease the wake fluctuations. A comparison of the traditional DBD plasma actuator and PSVGs shows that PSVGs achieve better control performance on the reduction of the recirculation bubble sizes and the Karman vortex shedding frequency in the wake at low speed because the PSVGs generate three-dimensional flow structures on the bluff body. Specifically, near the exposed electrodes, the freestream is entrained towards the model surface and flow separations hardly occur, whereas far from the exposed electrodes, streamwise vortices are induced, which hinder the formation of spanwise recirculation regions over the bluff body. Thus, the recirculation bubble regions behind the bluff body are reduced significantly and the vortex shedding in the wake is suppressed. This study suggests that PSVGs are a promising tool for conducting flow control in bluff body wakes. In the future, periodic control of PSVGs will be applied to explore the influence of the actuation frequencies on the control performance at high speed, including the drag coefficient comparison.

Acknowledgments

The authors are grateful for the financial support provided by the U.S. Office of Naval Research Global (under contract No. N62909-16-1-2161).

References

[1] J. H. Gerrard, J. H., "The mechanics of the formation region of vortices behind bluff bodies," *Journal of Fluid Mechanics*, Vol. 25, No. 02, 1966, pp. 401–413. doi:10.1017/s0022112066001721.

[2] Greenblatt, D., Göksel, B., Rechenberg, I., Schüle, C. Y., Romann, D., and Paschereit, C. O., "Dielectric Barrier Discharge Flow Control at Very Low Flight Reynolds Numbers," *AIAA Journal*, Vol. 46, No. 6, 2008, pp. 1528–1541. doi:10.2514/1.33388.

[3] Griffin, O. M., and Ramberg, S. E., "The vortex-street wakes of vibrating cylinders," *Journal of Fluid Mechanics*, Vol. 66, No. 03, 1974, pp. 553–576. doi:10.1017/s002211207400036x.

[4] Thomas, F. O., Kozlov, A., and Corke, T. C., "Plasma actuators for bluff body flow control," *3rd AIAA Flow Control Conference*, San Francisco, California, 2006. doi:10.2514/6.2006-2845.

[5] Thomas, F. O., Kozlov, A., and Corke, T. C., "Plasma actuators for cylinder flow control and noise reduction," *AIAA Journal*, Vol. 46, No. 8, 2008, pp. 1921–1931. doi:10.2514/1.27821.

[6] Corke, T. C., Enloe, C. L., and Wilkinson, S. P., "Dielectric Barrier Discharge Plasma Actuators for Flow Control," *Annual Review of Fluid Mechanics*, Vol. 42, No. 1, 2010, pp. 505–529. doi:10.1146/annurev-fluid-121108-145550.

[7] Shen, L., and Wen, C. Y., "Leading edge vortex control on a delta wing with dielectric barrier discharge plasma actuators," *Applied Physics Letters*, Vol. 110, No. 25, 2017, p. 251904. doi:10.1063/1.4989901.

[8] Jukes, Timothy and Segawa, Takehiko and Walker, Seth and Furutani, Hirohide and Iki, Norihiko and Takekawa, Shinya, "Active Separation Control over a NACA0024 by DBD Plasma Actuator and FBG Sensor," *Journal of Fluid Science and Technology*, Vol. 7, No. 1, 2012, pp. 39–52. doi:10.1299/jfst.7.39.

[9] Do, H., Kim, W., Mungal, M. G., and Cappelli, M. A., "Bluff Body Flow Separation Control using Surface Dielectric Barrier Discharges," *45th AIAA Aerospace Sciences Meeting and Exhibit*, Reno, Nevada, 2007. doi:10.2514/6.2007-939.

[10] Bhattacharya, S., and Gregory, J. W., "Optimum-wavelength forcing of a bluff body wake," *Physics of Fluids*, Vol. 30, No. 1, 2018, p. 015101. doi:10.1063/1.4999091.

[11] Jukes, Timothy N. and Segawa, Takehiko and Furutani, Hirohide, "Flow Control on a NACA 4418 Using Dielectric-Barrier-Discharge Vortex Generators," *AIAA Journal*, Vol. 51, No. 2, 2013, pp. 452–464. doi:10.2514/1.J051852.

[12] Wicks, M., Thomas, F. O., Corke, T. C., Patel, M., and Cain, A. B., "Mechanism of vorticity generation in plasma streamwise vortex generators," *AIAA Journal*, Vol. 53, No. 11, 2015, pp. 3401–3413. doi:10.2514/1.j053997.

[13] Kelley, C. L., Corke, T. C., Thomas, F. O., atel, M., and Cain, A. B., "Design and scaling of plasma streamwise vortex generators for flow separation control," *AIAA Journal*, Vol. 54, No. 11, 2016, pp. 3397–3408. doi:10.2514/1.j054950.

[14] Li, Yuwen and Nahon, Meyer and Sharf, Inna, "Airship dynamics modeling: A literature review," *Progress in Aerospace Sciences*, Vol. 47, No. 3, 2011, pp. 217–239. doi:10.1016/j.paerosci.2010.10.001.

[15] Dalla Longa, L.and Morgans, A. S.and Dahan, J. A., "Reducing the pressure drag of a D-shaped bluff body using linear feedback control," *Theoretical and Computational Fluid Dynamics*, Vol. 31, No. 6, 2017, pp. 567–577. doi:10.1007/s00162-017-0420-6.

[16] Forte, M., Jolibois, J., J.and Pons, Moreau, E., Touchard, G., and Cazalens, M., "Optimization of a dielectric barrier discharge actuator by stationary and non-stationary measurements of the induced flow velocity: application to airflow control," *Experiments in Fluids*, Vol. 43, No. 6, 2007, pp. 917–928. doi:10.1007/s00348-007-0362-7.

[17] Shen, L., Chen, Z., and Wen, C. Y., "Experimental investigation of the flow structure over a delta wing via flow visualization methods," *Journal of Visualized Experiments*, 2018. doi:10.3791/57244.

[18] Sciacchitano, Andrea and Wieneke, Bernhard, "PIV uncertainty propagation," *Measurement Science and Technology*, Vol. 27, No. 3, 2016, p. 084006. doi:10.1088/0957-0233/27/8/084006.

[19] Shen, L., Wen, C. Y., and Chen, H.-A., "Asymmetric Flow Control on a Delta Wing with Dielectric Barrier Discharge Actuators," *AIAA Journal*, Vol. 54, No. 2, 2016, pp. 652–658. doi:10.2514/1.j054373.